Materials Science & Engineering A 605 (2014) 236–243

Contents lists available at ScienceDirect

Materials Science & Engineering A

journal homepage: www.elsevier.com/locate/msea

Cryogenic treatments on AISI 420 stainless steel: Microstructure and mechanical properties

G. Prieto [a,*], J.E. Perez Ipiña [b], W.R. Tuckart [a]

[a] Tribology Group, Universidad Nacional del Sur/CONICET, Av. Alem 1253, 8000 Bahía Blanca, Argentina
[b] GMF UNComa/CONICET, Buenos Aires 1400, 8300 Neuquén, Argentina

ARTICLE INFO

Article history:
Received 11 October 2013
Received in revised form
12 March 2014
Accepted 14 March 2014
Available online 24 March 2014

Keywords:
Carbide precipitation
Hardness
Impact toughness
XRD

ABSTRACT

Cryogenic treatments have been employed over the last three decades in both tool and high-alloy steels to improve wear resistance, mainly through the transformation of retained austenite and the precipitation of fine carbides. The application of these treatments to low-alloy steels and even to non-ferrous materials is becoming the subject of several investigations, due to their potentiality to reduce wear.

This study was aimed at analyzing the microstructural changes and the effect of cryogenic treatments on hardness and impact toughness in martensitic AISI 420 stainless steel. X-ray diffraction (XRD) was employed for phase analysis and characterization, while carbide volume fraction, size and composition evaluation was measured by using scanning electron microscopy (SEM-EDX) and Energy Dispersive Spectrometry (EDS). Hardness was assessed with Vickers technique and the impact toughness was measured by means of Charpy's V-notch tests. Fracture surfaces were analyzed by scanning electron microscopy to evaluate the fracture micromechanisms.

In this study, it has been experimentally demonstrated that cryogenic treatments favors the precipitation of small carbides, which also present a more homogeneous size distribution. It was observed that this microstructural feature is responsible for the improvement in the mechanical properties of the material.

1. Introduction

Research made over the last three decades has indicated that the wear resistance of metallic alloys can substantially be improved by the application of cold treatments. This procedure usually consists in the addition of a cooling stage amidst conventional heat treatment. As a general rule, this cold stage is performed immediately after quenching. Those investigations focused primarily on both tool and high-alloy steels, where significant increases in wear resistance had been found [1,4,6]. The primary application of these treatments is to improve the wear resistance and the dimensional stability of stamps, die tools and motor blocks. More recently, they had spread widely along various industries and material families, being applied to power generation, valves, gears, motor racing parts, gun barrels and surgical and musical instruments [10]. New application fields for cryogenic treatments are under constant development, where their effects are being studied over the modification of fatigue behavior in steels [11,12]. The modification of deformation and the electrical properties of non-ferrous alloys, especially in copper, aluminum and magnesium have also became research subjects [13–15].

Cryogenic treatments are usually classified according to their dependence on the minimum temperature achieved during processing. Cold treatments (CT) are those where temperature is around 193–240 K, and dry ice is employed as coolant medium. In Shallow Cryogenic Treatments (SCT), specimens are cooled down to −80 °C, while in Deep Cryogenic Treatments (DCT) much lower temperatures are reached by using liquid nitrogen (−196 °C) or liquid helium (−269 °C) as cooling agents [4]. An important feature of cryotreatments is that they have a volumetric effect, meaning that changes have been made in the whole volume of the material, thus remaining unaltered after successive regrindings. Cryogenic treatment variables, like cooling rates and soaking times have been widely investigated, both for high-alloy and tool steels. Baldissera and Delprete [10] made a review of the state of the art of cryogenic treatments, reporting that prolonged soaking times, which are commonly ranging from 24 to 48 h and extremely slow cooling rates were the most commonly employed, in order to prevent crack formation. Molinari et al. [16] have suggested that the cooling rate should not exceed 20–30 °C/h and soaking times should be about 35 h. Stratton and Graff [18] have reported that a minimum of 24 h of soaking time is required at −196 °C and that using liquid helium (−269 °C) yielded no additional benefits compared to soaking in liquid nitrogen during deep cryogenic treatment of case hardened components.

* Corresponding author. Tel.: +54 291 4595156.
E-mail address: german.prieto@uns.edu.ar (G. Prieto).

http://dx.doi.org/10.1016/j.msea.2014.03.059
0921-5093/

Oppenkowski et al. [19] used a $L_{27}(3^{13})$ orthogonal array based on the Taguchi Design of Experiment (DOE) method to evaluate the influence of DCT variables on the effect over the mechanical and wear properties of an AISI D2 steel. Their results showed that the austenitising and the tempering temperatures were the most significant parameters, while holding time and heating rate had lower confidence levels and cooling rate had no significant effect. Following a similar approach by using Taguchi DOE, Darwin et al. [20] investigated the significance of cryogenic treatment parameters and their interactions over the wear resistance of a high-alloy martensitic stainless steel. In this case, they found that soaking temperature was the most significant parameter, which should be below −184 °C for optimal results. Soaking time and cooling rate were in the next places in their significance ranking. In the research work conducted by Akhbarizadeh et al. [21], the allowance of a stabilization time after DCT, as well as longer soaking times at shallow cryogenic temperature (40 h at −150 °C) improved wear resistance. This effect was attributed to the further transformation of retained austenite into martensite.

Extensive discussions have arisen regarding the mechanisms responsible for the changes in the mechanical properties of cryogenically treated steels. Several authors, including Barron [1], Da Silva et al. [2] and Das et al. [3] have reported the transformation of retained austenite into martensite as one of the main factors for wear resistance improvement, especially in high-alloy steels. In these kind of materials, the presence of gammagenic elements, like manganese, boron, molybdenum and chromium, depresses the martensite finish temperature deeply below room temperature. Because of this effect, high amounts of austenite can be found after heat treatment [16]. Cooling down the material at sub-zero temperatures after quenching is an effective way to transform this retained austenite into martensite, thereby increasing the resulting hardness and strength, as reported by Leskovšek et al. [9] and Tyshchenko et al. [26].

Another important phenomenon related to wear enhancement is the precipitation of small secondary carbides. Meng et al. [5,6] and Stratton et al. [17,18] focused their investigations in this subject. They found that cryogenic treatments generate the precipitation of a high amount of secondary carbides, with a reduction of the average particle size and a homogenization of particle size distribution.

Martensitic stainless steels have chromium as the main alloying element, with a content usually ranging from 12 to 17 wt%, while carbon is between 0.2 and 1.0 wt%. Nickel, molybdenum, vanadium, niobium, aluminum and copper are also added as alloying elements. Due to its high chromium content, these steels have excellent templability, allowing air quenching in some cases.

AISI 420 belongs to the family of martensitic stainless steels, having relatively low carbon content and around 12 wt% chromium. Due to its balance between mechanical properties and corrosion resistance, it is widely used in power generation, turbine blades, compressors, oil extraction, chemical, petrochemical and surgical equipment. Increasing its wear resistance would allow its utilization under more severe conditions [30].

The purpose of this research was to improve the hardness of a low-carbon AISI 420 stainless steel by means of cryogenic treatments. The microstructural modifications were assessed and correlated with the hardness and impact toughness variations of the material in order to discuss the possible mechanisms responsible for the modifications in these properties.

2. Experimental methods

2.1. Heat treatments

The material used in this research was AISI 420 stainless steel with a low carbon content. The chemical composition was determined by using a SPECTRO MAXX optic emission spectrometer and it is shown in Table 1, along with the reference composition taken from ASM Metal Handbook Volume 3 [41]. Carbon content was very close to the lower limit of the datasheet specification, which allows a carbon content up to 0.4 wt%.

Specimens were heated up to 830 °C, with a holding time of 10 min in order to achieve thermal equilibrium in the whole volume of the material. The heating continued until a temperature of 1030 °C was reached. Specimens were held at this temperature for 10 min to ensure complete austenization. Oil quenching was performed immediately afterwards. This whole procedure was performed in an argon atmosphere furnace in order to avoid oxidation and decarburation.

Quenched specimens were then lowered into a chamber containing liquid nitrogen at −196 °C. Soaking times were 1 h or 2 h. The following two cooling methods were employed: I. direct immersion in liquid nitrogen and II. a controlled process at a cooling rate of 0.45 °C/s. Once the soaking stage had been completed, specimens were extracted from the chamber in 10 min. Additionally, shallow cryogenic treatments (SCT) were performed at −40 °C and −80 °C with a holding time of 2 h and employing a cooling rate of 0.45 °C/s. Table 2 shows an overview of the applied heat treatments.

For the final stage of the heat treatment, specimens were tempered in an argon atmosphere at 410 °C in order to increase the material's toughness. Heating rate was established at 0.6 °C/s and the holding time was 10 min. Afterwards, specimens were cooled down inside the furnace. A representation of the thermal cycles applied is shown in Fig. 1.

After heat treatment, all specimens were grounded with abrasive silicon carbide waterproof papers up to 1500 grit and polished with an alumina powder water suspension, of 3 μm grain size.

2.2. Microstructural characterization

X-ray diffractometry was performed in order to identify present phases in the material. A PANALYTICAL X'PERT-MPD diffractometer was employed, using CuK_α radiation ($\lambda = 1.5405$ Å) at an acceleration potential of 40 kV. The diffraction angle ranged from

Table 1
AISI 420 chemical composition (wt%).

Element	AISI 420 datasheet (wt%)	Bar (wt%)
C	0.15 min	0.177
Cr	12.00–14.00	12.83
Si	1.00 max	0.55
Mn	1.00 max	0.76
P	0.04 max	0.05
S	0.03 max	0.017
Fe	Balance	Balance

Table 2
Description of applied heat treatments.

Identification	Description
CHT	Conventionally heat treated
DCT-1F	Cryogenically treated at −196 °C for 1 h. Direct LN immersion
DCT-2F	Cryogenically treated at −196 °C for 2 h. Direct LN immersion
DCT-1C	Cryogenically treated at −196 °C for 1 h. 0.45 °C/s Cooling rate
DCT-2C	Cryogenically treated at −196 °C for 2 h. 0.45 °C/s Cooling rate
SCT-1	Shallow cryogenically treated at −40 °C for 2 h. 0.45 °C/s Cooling rate
SCT-2	Shallow cryogenically treated at −80 °C for 2 h. 0.45 °C/s Cooling rate

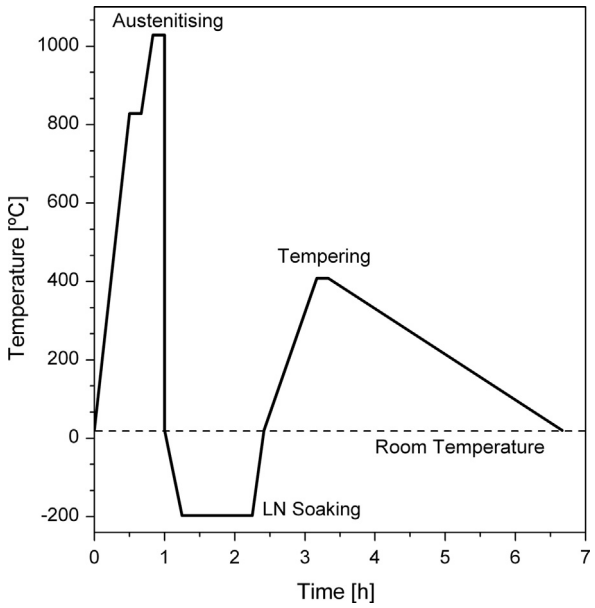

Fig. 1. Schematization of applied heat treatments.

20 to 120°, with a 0.02° step at a speed of 0.06°/min. The diffractometer was equipped with a graphite diffracted-beam collimator and a programmable receiving slit of 0.2 mm, a divergence slit of 0.4° and an incident and collecting slit of 1°. It also had a collecting slit, in order to improve resolution and to minimize the effect of iron X-ray fluorescence that can interfere with the diffracted peaks. One specimen of each heat treatment was analyzed with this technique over a square scanned region of 15×15 mm^2.

Scanning electron microscopy images, obtained with a CARL ZEISS EVO 40 XVP scanning electron microscope, were examined to quantitatively estimate the amount and size of precipitated second phase particles. The spot counting analyses were all made over images of the same size and magnification level. In order to measure the diameter of precipitated carbides, a square grid that consisted of 560 quadrants of 3.6 μm side was overlapped to the images. Measurements were made over 56 randomly selected quadrants. Afterwards, carbide size distribution was estimated, as well as carbide volume fraction by means of stereological relationships. More than 900 carbide particles were considered for these calculations.

Specimen preparation for SEM consisted in polishing the specimens progressively with abrasive paper up to grit 2500. Final polishing was made with an alumina suspension (particle size: 3 μm). Afterwards a Marble reagent (10 g $CuSO_4$ in 50 ml HCl and 50 ml water) was applied during 5 s in order to reveal the microstructural features.

An Energy Dispersive Spectrometry (EDS) with Thin Film Standardless Quantitative Analysis was performed in the precipitated particles, so as to identify them. This analysis was made by using a JEOL JEM-2100 transmission electron microscope. The acceleration voltage applied was 200 kV at a magnification level of 30,000 ×.

2.3. Mechanical properties evaluation

The hardness of tempered specimens was evaluated by using an OSHMA HV-50A Vickers durometer. Measurements were performed with 98 N of applied load during 7 s over polished specimens. 25 hardness measurements were made for each heat treatment.

Impact toughness was assessed by mean of Charpy V-Notch tests. Specimen geometry and testing conditions met the requirements of ASTM E23-02 [50] standard for a regular size specimen ($55 \times 10 \times 10$ mm^3). Specimens were machined before heat treatment using a mill and finished with a grinding wheel, while the notchs were made using an electroerosion process, once the heat treatments were completed. Final polishing using 600 mesh abrasive paper was made prior testing.

Impact tests were performed by using an AVERY-DAVISON CHARPY PENDULUM, with an impact energy capability of 300 J at 5 m/s. Tests were made on 7 specimens of each DCT treatment. Fracture surfaces were examined by using a PHILIPS 515 scanning electron microscope. SCT specimens were not considered for Charpy tests.

Both hardness and impact toughness data were processed using the statistical software INFOSTAT Ver 2012e [51] in order to evaluate the changes in the response of the material due to cryogenic processing. ANOVA tests and paired comparisons (Fisher's LSD) were performed over experimental data at a 0.05 significance level.

3. Results

3.1. Microstructural characterization

The X-ray diffraction patterns, presented in Fig. 2 correspond to CHT and DCT-2C specimens. They showed characteristic martensitic peaks [33], but there is no evidence of peaks corresponding to austenite [34]. Therefore, it can be inferred that the volume fraction of austenite phase is below the detection threshold of the equipment, which is ≈3% [31], being this value sensitive to several diffractometer parameters and its data collection systems. Reported error levels are usually around 5% [35]. On closer examination the diffraction patterns show peak broadening and shifting, as it can be seen in Fig. 3.

Carbide average size and distribution varied according to the heat treatment that was applied, as it can be seen in Fig. 4a and b respectively. Scanning electron microscopy images showed in all

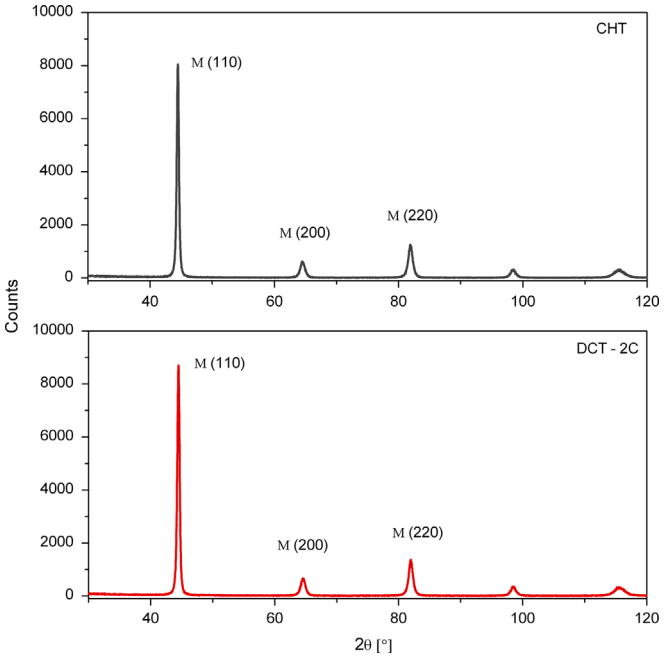

Fig. 2. X-ray diffraction patterns for CHT and DCT-2C specimens.

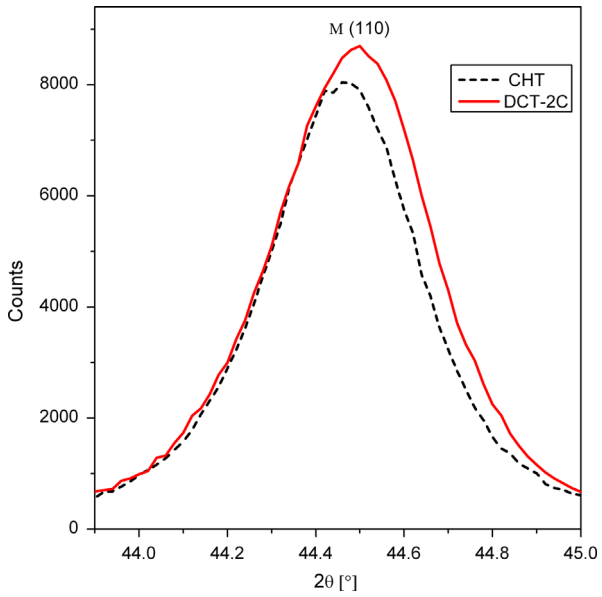

Fig. 3. Martensite (110) peak broadening due to application of cryogenic treatment.

cases a microstructure consisting of a martensitic matrix and precipitated globular carbides (Fig. 5).

The EDS analysis of precipitated second phase particles identified them as secondary carbides. The EDS analysis of a M_7C_3 carbide is shown in Fig. 6a, along with its quantitative analysis, presented in Table 3.

As it could be seen from SEM images, DCT specimens showed reduced carbide size and a refinement of its size distribution. The image analysis evidenced a strong increase in the number of small carbides in specimens with 2 h of soaking time subjected to controlled cooling compared to those conventionally treated. As it can be seen in Fig. 7, in DCT-2C specimens, almost 70% of detected carbides had diameters below 0.4 μm. Furthermore, carbide volume fraction, which was estimated by means of the relationship between the analyzed area and the carbide area, lowered from 17% in CHT specimens to 12% in DCT-2C specimens.

CHT specimens showed a size distribution that was more heterogeneous. This means that they had a significant amount of particles for each size classification. Carbide size diminished with longer soaking times and small particle population (carbide diameter below 0.4 μm) markedly increased. This effect can be observed in Fig. 7, where both the number of carbides classified by size and the cumulative percentage for specimens with different heat treatments are presented in a double *Y* axis plot.

3.2. Mechanical properties

DCT-2C specimens had a statistically significant ($p < 0.01$) difference in their mean hardness value. The increment measured in these specimens was in the order of 30 Vickers hardness points (5%) when taking CHT specimens as baseline. Fig. 8 displays the output of the Fisher's LSD test, where the mean hardness value of each treatment is presented in decreasing order, along with its error bars and difference identification. Means with the same letter are not statistically different at the selected significance level. The absence of a significant difference between the mean value of SCT specimens when compared to CHT ones led us to dismiss these specimens from further analysis, such as Charpy tests and SEM examination.

By using the same combination of ANOVA and Fisher's LSD tests, absorbed energy in Charpy tests was analyzed. DCT-2C specimens evidenced an increase in the mean value of absorbed

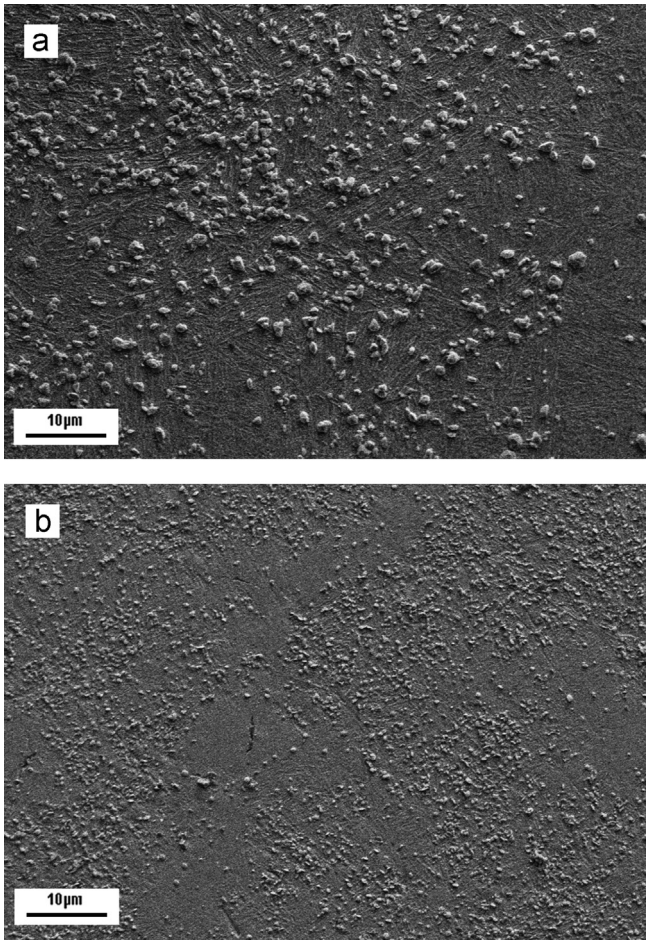

Fig. 4. SEM images at 3000 × : (a) CHT specimen and (b) DCT-2C specimen.

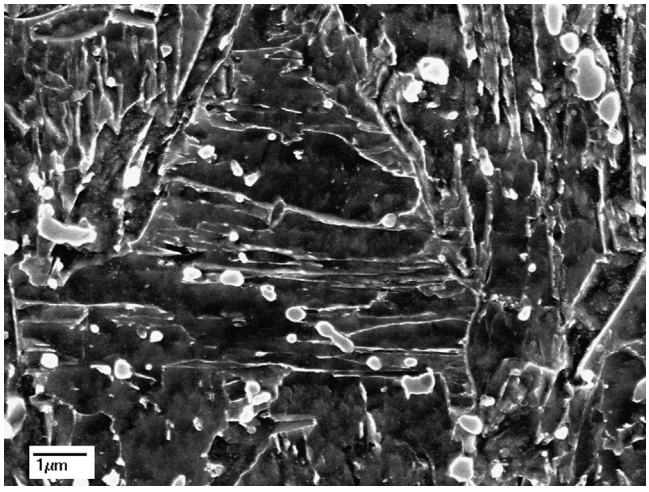

Fig. 5. SEM image at 10,000 × of a DCT-2C specimen showing globular carbides.

energy of 10%, as it can be seen in Fig. 9. The rest of the treatments showed no statistically significant difference between their mean values. In this case, due to the diverse variation sources involved in Charpy testing (number of tests, specimen preparation and geometry, experimental procedure, etc.), the statistical power of ANOVA tests was relatively low, showing a *p*-value of ≈ 0.1.

Fracture surface examination performed near the notch tip, showed a mixture of cleavage facets and small dimples in CHT specimens, while DCT-2C specimens had a higher amount of dimples and almost no cleavage facets. Fig. 10 shows a SEM fractography

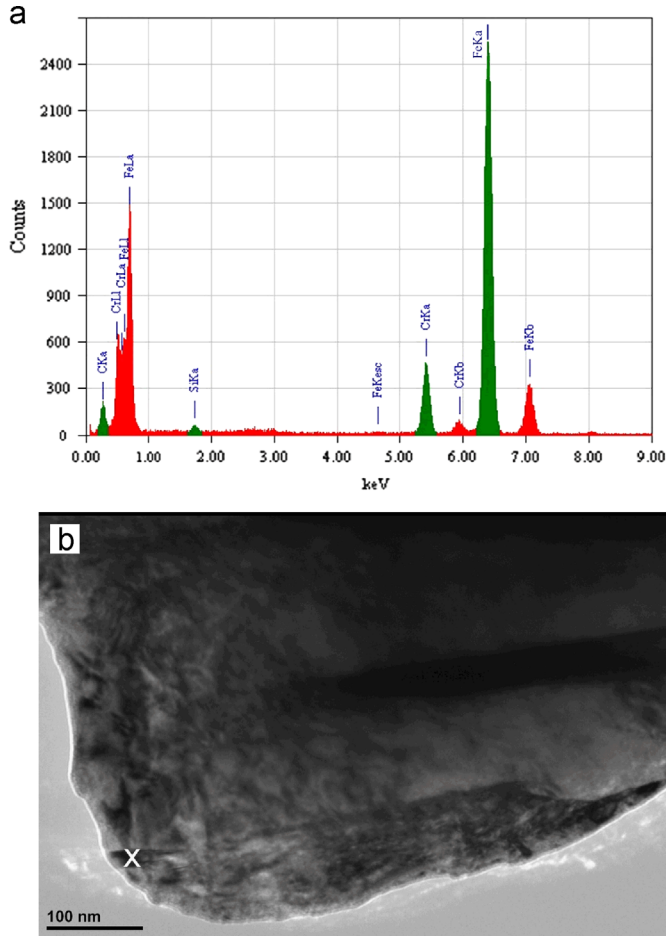

Fig. 6. (a) EDS analysis of a M_7C_3 carbide and (b) TEM image at 30,000×. The reported EDS analysis was performed in the marked spot.

Table 3
Thin Film Standardless Quantitative Analysis of a M_7C_3 carbide.

Element	Energy [keV]	Counts	Mass%	Atom %
C	0.277	1718	9.01	31.22
Si	1.739	327	0.4	0.59
Cr	5.411	6.587	11.5	9.21
Fe	6.398	40.781	79.09	58.97

of a DCT-2C specimen, where a dimpled surface can be observed. It can also be noted that there are second phase particles located at the bottom of dimples.

4. Discussion

4.1. On the selection of cryogenic treatment parameters

In our present study, conventional heat treatment variables, such as austenitising and tempering temperatures were selected at fixed levels according to recommendations given by several handbooks [41,42] and cryogenic treatment parameters, like soaking time and cooling rate were varied, without statistically analyzing their relative significance over the modification of mechanical properties. The fact that sub-zero treatments had no significant effect over hardness (Fig. 8), at least for the selected soaking times, seems to support Darwin et al. [20] results. As shown in our X-ray diffraction results, we have found that retained austenite volume fractions are below the diffractometer detection limit even for CHT specimens (Fig. 2), thus letting us infer that stabilization periods and prolonged soaking times are of little significance for the heat treatment of AISI 420 stainless steel.

It is interesting to point out that recent developments regarding the computational simulation of cryogenic treatments are under progress [40], where the cooling behavior and temperature evolution of a cold work die steel soaked in liquid nitrogen were studied by using finite element simulation. Advancements in this

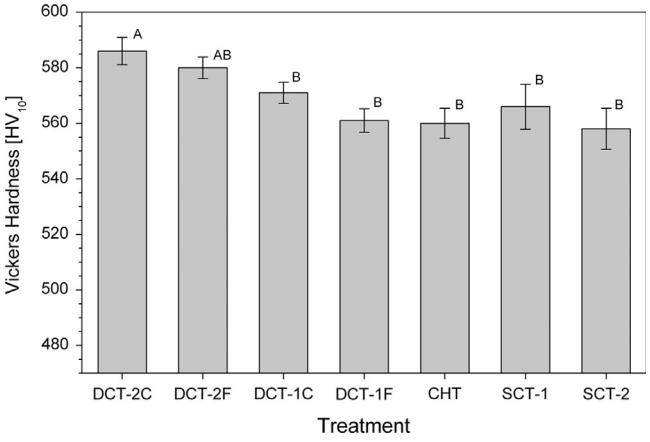

Fig. 8. Hardness mean value after heat treatment.

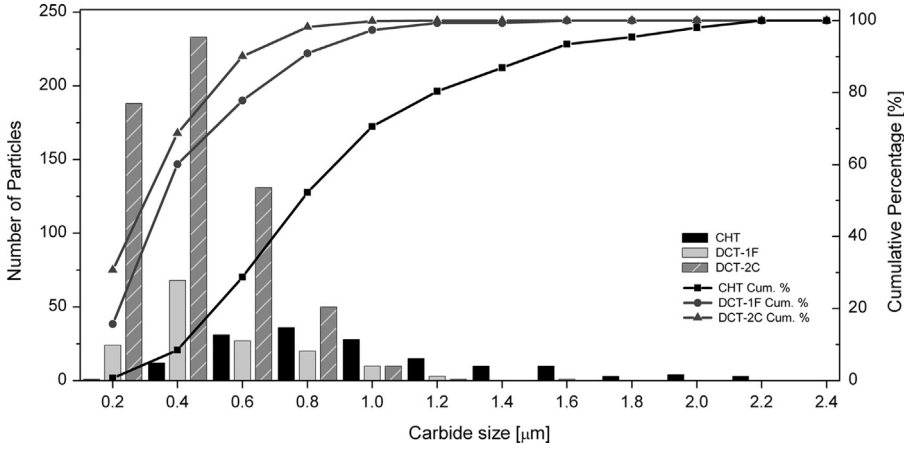

Fig. 7. Estimation of carbide size distribution.

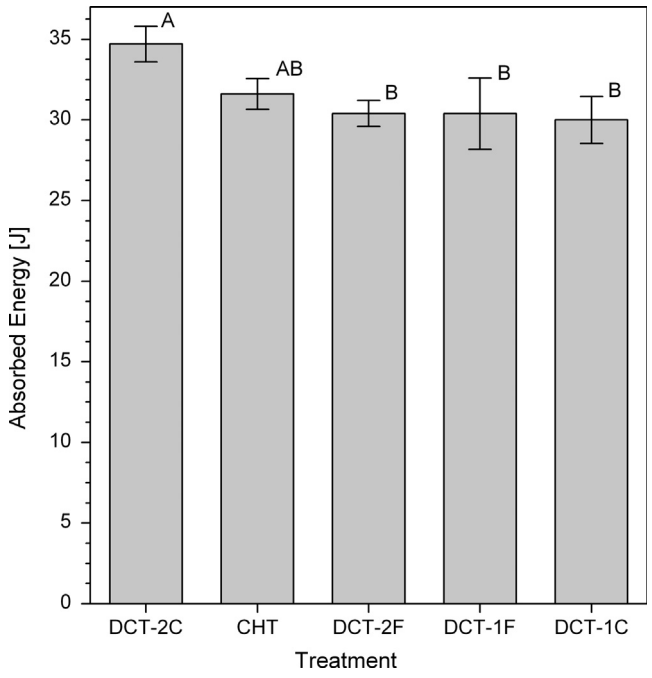

Fig. 9. Absorbed energy during impact mean value comparison.

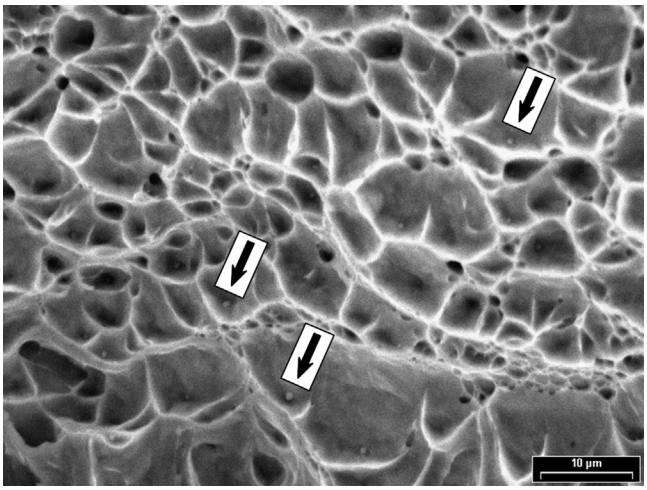

Fig. 10. SEM image at 5000× of fracture surface from a DCT-2C specimen. Arrows indicates the presence of carbides located at the bottom of dimples.

field will lead to a better understanding of the complex thermal and metallurgical dynamics involved in cryogenic treatments.

Since AISI 420 steel is far more ductile than HSS and tool steels that are used in most of the cryogenic-related investigations, it is more resistant to cracking during cooling [43]. Stratton [17] reported that both cooling and heating rates are only important to avoid cracking but are not critical for carbide formation. Therefore, we could apply faster cooling rates without compromising the mechanical integrity of the specimens. However, it can be seen in Fig. 9 that rapid cooling eliminated the absorbed energy improvement. Therefore, controlled cooling is recommended for DCT in AISI 420 stainless steel.

4.2. Variation of the strain state of martensite

The X-ray diffractograms showed no evidence of substantial amounts of retained austenite. This result is consistent with the fact that AISI 420 is an air-quenching steel. TTT diagrams for this alloy show a delay of more than 15 min until the appearance of the perlitic nose during cooling [42]. As oil quenching was performed, it was expected that retained austenite volume was indeed very low.

When comparing the X-ray diffractograms between cryogenically and conventionally treated specimens, it can be observed that diffraction peaks are broader in the case of DCT specimens. Research conducted by Warren and Averbach [37] and Williamson and Hall [36] had reported that higher strain states resulted in broader peaks in the X-ray diffractograms. Similarly, Pešička et al. [38] reported that martensitic shear created dislocations that helped to accommodate high internal stresses, thus leading to broader XRD profiles. In a more recent study, Xu et al. [39], showed that martensite exposed to cryogenic temperatures had increased tetragonality and full width at half maximum (FWHM) values compared to control group. Therefore, the peak broadening which was evidenced in cryogenically treated specimens (Fig. 3) can be attributed to both an increase in the strain state of the material and in the dislocation population density, generated during the cryogenic cooling stage of the heat treatment.

Those phenomena are directly related to heterogeneous stress distributions that can be acting as a driving force for the precipitation of smaller carbides, as it can be seen in Fig. 4b. This latter hypothesis had also been proposed by Meng et al. [5] and Collins and Dormer [7]. The study conducted by Tyschenko et al. [26] by using a combination of Mössbauer spectroscopy, TEM and XRD, supported the hypothesis that plastic deformation during martensitic transformation at low temperatures is a key factor for the formation of carbon clusters that serve as nucleation sites for fine carbides. The martensitic transformation at low temperatures is accompanied by plastic deformation due to the volume effect of the martensitic transformation, which leads to the capture of immobile carbon atoms by gliding dislocations, generating carbon clusters. During tempering, these carbon clusters serve as nucleation sites for the precipitation of fine carbides. Tyshchenko et al. [26] proved this capture effect by the gliding dislocations by means of internal friction measurements.

4.3. Reduction of average carbide size

In several studies performed by Das et al. [3,22,23] an average carbide size reduction after the application of cryogenic treatments was reported. A mean spherical carbide diameter reduction from 0.5 to 0.3 µm (34%) was found in [23] and similar figures were reported in [22]. Our results showed a much stronger size reduction. CHT specimens had a mean carbide diameter of 0.9 µm, while in DCT-2C specimens it was of 0.4 µm, accounting for a diameter reduction of 145%. It is interesting to point out that the diameter of carbides in cryogenically treated specimens reported in [22,23] and in our study converged towards a very similar value around 0.3–0.4 µm.

4.4. Carbide distribution

When analyzing carbide distribution, the increase in amount of carbides is consistent with the results given by Huang et al. [29] and Das et al. [3,22,23]. The quantity of particles below 1 µm has greatly been improved after DCT and the size distribution has become more concentrated around the sub-micron scale as it can be seen in Fig. 7. These phenomena are also followed by a reduction in the maximum carbide size detected in DCT specimens. Therefore the cryogenic treatment of AISI 420 steel specimens refined the secondary carbides, increased their amount and led to their more uniform distribution in the microstructure.

The decrease from 17% to 12% in carbide volume fraction that was reported above let us infer that the application of cryogenic treatments to AISI 420 stainless steel generates a different effect

over secondary carbides than the reported ones in several studies. For example, Das et al. [22,23], found values higher up to 11% in this feature in cryogenically treated specimens. In turn, Vahdat et al. [24], reported markedly increases in secondary carbide volume fraction in specimens with variable soaking times at −196 °C, ranging from 142% for specimens with 24 h soaking time to 1180% for specimens with 48 h at −196 °C. This difference in behavior could be related to the fact that AISI 420 has a much lower amount of carbon than the high-alloy steels studied in [22–24]. Therefore tempered martensite could be retaining a higher amount of carbon in solid solution that does not precipitates as secondary carbides during tempering.

It is also interesting to highlight that there are several procedures to establish the characteristics of carbide population. The combination of SEM images and image processing software seems to lead to fairly accurate results, taking into account even small particles that would have been omitted if optical microscopy had been used instead.

The transmission electron microscopy has proved to be a very powerful tool to analyze the precipitation of secondary carbides. Several research groups used this technique to investigate the effect of cryogenic treatments on their precipitation behavior and characteristics. Yun et al. [25] were able to find ultrafine carbides, precipitated into the martensitic matrix. Those carbides were very small in size, ranging in the order of 20–60 Å, and they were found segregated at the twin crystal surfaces while studying tool steels with DCT. Meng et al. [5,6] not only found small spherical carbides particles, but they also reported a change in the distribution of those particles, being more numerous and evenly distributed in the tempered matrix. Average particle size ranged between 0.3 and 0.5 μm. These results are in strong agreement with those reported in this study. However, it would be interesting to perform a thoroughly TEM examination of AISI 420 specimens with DCT, to deepen understanding of the precipitation of second phase particles.

Meng et al. [5] concluded that the mechanisms responsible for the wear resistance improvement were the change in the carbide distribution and the recovery of martensite, rather than the removal of retained austenite. As stated at the beginning of this section, XRD examination determined that retained austenite volume is below 3% even for CHT specimens, thus leaving carbide precipitation as the main microstructural modification in the AISI 420.

4.5. Hardness evaluations

Increases in hardness level of cryogenically treated materials have been reported in the majority of the literature. Das et al. [3] declared improvements in bulk hardness due to cold treatment ranging from ~3% to ~8% for an AISI D2 tool steel. The highest level of improvement corresponded to DCT specimens, and it was related to a reduction in retained austenite and to the precipitation of secondary carbides. Das and Ray [23] reported a moderate increase of the bulk hardness of a cryogenically treated AISI D2 steel. DCT specimens showed a 4% hardness increase compared to those conventionally heat treated. Additionally, they pointed out that the hardness increase is directly related to the lowest temperature achieved during the cryogenic stage. Molinari et al. [16] reported that cryogenic treatments generated hardness enhancements of 6% and 3% for AISI M2 and H13 tool steels, respectively in comparison with conventional heat treatment. Yun et al. [25] stated that deep cryogenic treatments enhances the bulk hardness of high-speed steels by 3% with reference to conventional heat treatment.

Collins and Dormer [8] studied the effect of shallow and deep cryogenic treatments on AISI D2 tool steel with different austenitising temperatures. Their results showed that deep cryogenic treatments avoided hardness loss at high austenitising temperatures due to the transformation of retained austenite to martensite during deep cryogenic treatment. DCT specimens were 20% harder than specimens austenitized at 1150 °C, while this difference was not significant with austenitising temperatures below 1000 °C. The precipitation of a finer distribution of carbides was considered as the factor that was responsible for toughness and wear resistance increases. Yun et al. [25] had reported increases in both room temperature and red hardness of high-speed steels. This latter enhancement was due to the precipitation of ultrafine carbides.

Therefore the hardness enhancement found in specimens with 2 h soaking time of 5% and 4% for controlled cooling (DCT-2C) and direct immersion (DCT-2F) respectively (Fig. 8) are in close agreement with those previously cited even though the transformation of retained austenite is not present in AISI 420 due to its high templability. Thus hardness increase in DCT specimens of AISI 420 can be attributed to the following facts: I. the precipitation of small secondary carbides, II. their finer distribution along the volume of the material and III. the higher strain state in the martensite.

4.6. Impact toughness evaluations

Regarding impact toughness, Saucedo-Muñoz et al. [44], while evaluating the fracture toughness by means of Charpy V-Notch testing of austenitic stainless steels for superconducting magnets, found that fracture energy decreased with increasing precipitate volume fraction. Tsuchiyama et al. [45,46] analyzed the effect of partial solution treatments on martensitic stainless steels. The isothermal aging promoted the precipitation of finely dispersed carbide particles within the matrix. This feature was responsible for the decrease in the ductile–brittle transition and for the increase in the upper shelf energy in comparison with the base material.

The results of Charpy V-notch impact tests presented in Fig. 9 provided a first approach to the effect of cryogenic treatments and its influence in fracture behavior, though fracture toughness tests should be performed in our future research efforts. The overall results showed that DCT-2C specimens evidenced an increase in impact toughness of 10% and a stronger presence of dimples in fractographies in comparison with CHT specimens. DCT-2C specimens had both the smallest average carbide size and the lowest carbide volume fraction, thus following a similar tendency to the one presented by Saucedo-Muñoz et al. [44] and Tsuchiyama et al. [45,46].

Das et al. [48] reported that the degree of reduction in fracture toughness for cryogenically treated AISI D2 steel varies with the types of sub-zero treatments. The lowest reduction, which was 7%, corresponded to deep cryogenically treated specimens, and it was attributed to a more refined carbide distribution in comparison with shallow cryogenic and cold-treated specimens. Therefore, reducing carbide size and improving their spatial distribution are key factors so as to prevent toughness loss when cryogenic treatments are applied. The impact toughness increase informed earlier in our cryogenically treated specimens might be related to the fact that the carbide size reduction was greater than the one obtained in [48], being in this case 22%, while for the cryogenically treated AISI 420 specimens that we tested it reached 145%.

Da Silva et al. [2] reported a 43% enhancement in impact toughness of DCT high-speed steels compared to conventionally treated specimens. Those results were attributed both to the transformation of retained austenite and to the precipitation of ultrafine carbides, the latter being considered as the key factor for changes in properties. Yun et al. [25] reported the same increment

in impact toughness (43%) for W18Cr4V steel, while W6Mo5Cr4V2 showed a 58% increase in this feature.

Molinari et al. [16] have found that no significant modification in impact toughness is achieved when the cryogenic stage is made after tempering, but when it is performed after quenching, absorbed energy decrease in the order of 24%.

It is important to notice that fractured surfaces (Fig. 10) should have been evaluated at several positions [47] in order to fully assess the acting mechanisms and the different behavior between DCT and conventionally heat treated material. This is due to the fact that even though dimples have been found near the notch edge during SEM examination of fracture surfaces, cleavage facets has also been detected in the region of crack propagation, before complete fracture. Bensely et al. [49] reported a reduction in tensile strength for DCT specimens over CHT of 9% in a case carburized steel, even though SEM analysis of fractured surfaces showed the same proportion of dimples and flat facets (50% each) in both groups of specimens.

5. Conclusions

- Cryogenic treatments can be applied to a low carbon stainless steel in order to generate modifications in microstructural and mechanical properties. In this work, deep cryogenic treatments increased the strain state in the martensite, leading to the precipitation of a higher amount of smaller secondary carbides with a more uniform distribution. Volume fraction of retained austenite after tempering was not significant, even for conventionally treated material.
- Soaking times of 2 h were enough to achieve both a hardness improvement of 5% and an increase in absorbed energy during impact of 10%. Material soaking at sub-zero temperatures yielded no significant difference in hardness when compared to CHT material. Thus, deep cryogenic temperatures need to be reached. Even though AISI 420 stainless steel can sustain faster cooling rates than conventional tool steels, direct immersion in liquid nitrogen is not recommended.

Acknowledgments

The authors wish to express herein their appreciation for the support given by the Engineering Department of Universidad Nacional del Sur and CONICET, as well as to Gustavo Montesi, Dr. Marcelo Gines CINI TENARIS and Dr. Darja Jenko IMT-Slovenia, for their valuable contributions to this paper.

References

[1] R.F. Barron, Cryogenics 22 (1982) 409–413.
[2] F.J. Da Silva, S.D. Franco, Á.R. Machado, E.O. Ezugwu, A.M. Souza, Wear 261 (2006) 674–685.
[3] D. Das, A.K. Dutta, K.K. Ray, Mater. Sci. Eng. A 527 (2010) 2182–2193.
[4] D. Das, A.K. Dutta, K.K. Ray, Mater. Sci. Eng. A 527 (2010) 2194–2206.
[5] F. Meng, T. Kohsuke, R. Azuma, H. Sohma, ISIJ Int. 34 (1994) 205–210.
[6] F. Meng, K. Tagashira, H. Sohma, Scr. Metall. Mater. 31 (1994) 865–868.
[7] D.N. Collins, J. Dormer, Heat Treat. Met. 24 (1997) 71–74.
[8] D.N. Collins, J. Dormer, Int. Heat Treat. Surf. Eng. 2 (2008) 150–154.
[9] V. Leskovšek, M. Kalin, J. Vižintin, Vacuum 80 (2006) 507–518.
[10] P. Baldissera, C. Delprete, Open Mech. Eng. J. 2 (2008) 1–11.
[11] P. Baldissera, C. Delprete, Mater. Des. 31 (2010) 4731–4737.
[12] P. Baldissera, Mater. Des. 30 (2009) 3636–3642.
[13] K.M. Asl, A. Tari, F. Khomamizadeh, Mater. Sci. Eng. A 523 (2009) 27–31.
[14] K. Gu, H. Zhang, B. Zhao, J. Wang, Y. Zhou, Z. Li, Mater. Sci. Eng. A 584 (2013) 170–176.
[15] J. Liu, G. Li, D. Chen, Z. Chen, Chin. J. Aeronaut. 25 (2012) 931–936.
[16] A. Molinari, M. Pellizzari, S. Gialanella, G. Straffelini, K.H. Stiasny, J. Mater. Process. Technol. 118 (2001) 350–355.
[17] P. Stratton, Mater. Sci. Eng. A 449 (2007) 809–812.
[18] P. Stratton, M. Graf, Cryogenics 49 (2009) 346–349.
[19] A. Oppenkowski, S. Weber, W. Theisen, J. Mater. Process. Technol. 210 (2010) 1949–1955.
[20] J. Darwin, D. Mohan Lal, G. Nagarajan, J. Mater. Process. Technol. 195 (2008) 241–247.
[21] A. Akhbarizadeh, A. Shafyei, M. Golozar, Mater. Des. 30 (2009) 3259–3264.
[22] D. Das, A.K. Dutta, K.K. Ray, Cryogenics 49 (2009) 176–184.
[23] D. Das, K.K. Ray, Mater. Sci. Eng. A 541 (2012) 45–60.
[24] S.E. Vahdat, S. Nategh, S. Mirdamadi, Mater. Sci. Eng. A 585 (2013) 444–454.
[25] D. Yun, L. Xiaoping, X. Hongshen, Heat Treat. Met. 3 (1998) 55–59.
[26] A.I. Tyshchenko, W. Theisen, A. Oppenkowski, S. Siebert, O.N. Razumov, A.P. Skoblik, V.A. Sirosh, et al., Mater. Sci. Eng. A 527 (2010) 7027–7039.
[29] J. Huang, Y. Zhu, X. Liao, I. Beyerlein, M. Bourke, T. Mitchell, Mater. Sci. Eng. A 339 (2003) 241–244.
[30] A.N. Isfahany, H. Saghafian, G. Borhani, J. Alloys Compd. 509 (2011) 3931–3936.
[31] R.W. Hinton, J. Test Eval. 15 (1987) 95–100.
[33] Database of the International Centre for Diffraction Data (ICDD) 31-0619.
[34] Database of the International Centre for Diffraction Data (ICDD) 6-0696.
[35] R.E. Dinnebier, S.J.L. Billinge, Powder Diffraction: Theory and Practice, first ed., Royal Society of Chemistry, Cambridge, 2008.
[36] G.K. Williamson, W.H. Hall, Acta Metall. Mater. 1 (1953) 22–33.
[37] B.E. Warren, B.L. Averbach, J. Appl. Phys. 21 (1950) 595.
[38] J. Pešička, R. Kužel, A. Dronhofer, G. Eggeler, Acta Metall. Mater. 51 (2003) 4847–4862.
[39] N. Xu, G.P. Cavallaro, A.R. Gerson, Mater. Sci. Eng. A 527 (2010) 6822–6830.
[40] J. Li, L. Tang, S. Li, X. Wu, Mater. Des. 47 (2013) 653–666.
[41] F. Hardesty, Metals Handbook, 9th ed., Handbook Committee, ASM, Metals Park, OH, USA, 1980.
[42] G. Istrati, Manual de los Aceros Inoxidables, Alsina, Buenos Aires, 1961.
[43] G. Pender, A.O. Lucaioli, Actas del Congreso Binacional Sam Conamet: Jornadas MEMAT, 2005, 221–225.
[44] M.L. Saucedo-Muñoz, Y. Watanabe, T. Shoji, H. Takahashi, Cryogenics 40 (2000) 693–700.
[45] T. Tsuchiyama, S. Takaki, ISIJ Int. 39 (1999) 202–208.
[46] T. Tsuchiyama, Y. Ono, S. Takaki, ISIJ Int. 40 (2000) 184–188.
[47] B. Tanguy, J. Besson, R. Piques, A. Pineau, Eng. Fract. Mech. 72 (2005) 49–72.
[48] D. Das, R. Sarkar, A.K. Dutta, K.K. Ray, Mater. Sci. Eng. A 528 (2010) 589–603.
[49] A. Bensely, D. Senthilkumar, D. Mohan Lal, G. Nagarajan, A. Rajadurai, Mater. Charact. 58 (2007) 485–491.
[50] ASTM Standard E23, Standard Test Methods for Notched Bar Impact Testing of Metallic Materials, ASTM International, West Conshohocken, PA, 2002.
[51] J.A. Di Rienzo, F. Casanoves, M.G. Balzarini, L. Gonzalez, M. Tablada, C.W. Robledo, InfoStat (Version 2012) [Computer Software], Universidad Nacional de Córdoba, Córdoba, Argentina, 2012 (Retrieved from: ⟨http://www.infostat.com.ar⟩).